

Velocity anisotropy in tidally limited star clusters

Maria A. Tiongco^{1*}, Enrico Vesperini¹, and Anna Lisa Varri²

¹*Department of Astronomy, Indiana University, Bloomington, IN 47405, USA*

²*School of Mathematics and Maxwell Institute for Mathematical Sciences, University of Edinburgh, Edinburgh EH9 3JZ, UK*

10 November 2015

ABSTRACT

We explore the long-term evolution of the anisotropy in the velocity space of star clusters starting with different structural and kinematical properties. We show that the evolution of the radial anisotropy strength and its radial variation within a cluster contain distinct imprints of the cluster initial structural properties, dynamical history, and of the external tidal field of its host galaxy. Initially isotropic and compact clusters with small initial values of the ratio of the half-mass to Jacobi radius, r_h/r_J , develop a strong radial anisotropy during their long-term dynamical evolution. Many clusters, if formed with small values of r_h/r_J , should now be characterized by a significant radial anisotropy increasing with the distance from the cluster centre, reaching its maximum at a distance between $0.2 r_J$ and $0.4 r_J$, and then becoming more isotropic or mildly tangentially anisotropic in the outermost regions. A similar radial variation of the anisotropy can also result from an early violent relaxation phase. In both cases, as a cluster continues its evolution and loses mass, the anisotropy eventually starts to decrease and the system evolves toward an isotropic velocity distribution. However, in order to completely erase the strong anisotropy developed by these compact systems during their evolution, they must be in the advanced stages of their evolution and lose a large fraction of their initial mass. Clusters that are initially isotropic and characterized by larger initial values of r_h/r_J , on the other hand, never develop a significant radial anisotropy.

Key words: globular clusters

1 INTRODUCTION

A complete characterization of globular cluster dynamical properties requires information on both the cluster structure and kinematics. Observational studies have extensively explored the internal spatial structure of Galactic clusters (see e.g. Djorgovski & Meylan 1994; McLaughlin & van der Marel 2005; Miocchi et al. 2013) and significant efforts have been invested in theoretical investigations aimed at understanding the cluster structural evolution and at providing numerical and analytical models for the interpretation of observational data (see e.g. Heggie & Hut 2003 and references therein).

The observational study of the internal kinematical properties of globular clusters, on the other hand, is much more challenging. After a few early efforts (see e.g. Gunn & Griffin 1979; Lupton et al. 1987; Pryor & Meylan 1993; Gebhardt et al. 1995; van Leeuwen et al. 2000; see also Meylan & Heggie 1997 and references therein), only recently observational investigations have started to provide more extensive information on globular cluster kinematics thanks to, for example, ESO/VLT radial velocity (see e.g. Bellazzini et al. 2012; Lanzoni et al. 2013; Lardo et al. 2015) and HST proper motion measurements (Bellini et al. 2014; Watkins et al. 2015). Forthcoming measurements from the Gaia astrometric

mission will soon provide a wealth of new data and further enrich the observational study of cluster kinematics (see e.g. Pancino et al. 2013; Sollima et al. 2015).

A more detailed knowledge of clusters' kinematics allows to address a number of fundamental questions concerning their dynamics and stellar content such as, for example, the strength of internal rotation, the possible link between internal rotation and cluster morphology (see e.g. Bianchini et al. 2013; Fabricius et al. 2014; Kacharov et al. 2014), the presence of intermediate-mass black holes (see e.g. Lützendorf et al. 2011; Anderson & van der Marel 2010; Lanzoni et al. 2013), and the possible differences in the dynamical history of the multiple stellar populations observed in many clusters (Richer et al. 2013; Bellini et al. 2015).

In this paper we present the results of a survey of N -body simulations following the long-term evolution of systems with a broad range of different initial structural and kinematical properties and including the effects of an external tidal field. Our study is focused on the evolution of the anisotropy in the velocity space and aimed at exploring the connection between the evolution of the velocity anisotropy and the cluster initial conditions and dynamical history. We will show that different initial structural properties, different evolutionary phases, and the external tidal field leave distinct imprints on the strength of the velocity distribution anisotropy and its radial variation within a cluster. The results obtained further emphasize the wealth of crucial dynamical information contained in

* E-mail: mtiongco@indiana.edu

Table 1. Simulation Information.

Model ID	$(r_h/r_J)_i$	$(r_t/r_J)_i$
KF1	0.116	1.0
KF075	0.087	0.75
KF05	0.058	0.5
KF025	0.029	0.25
KF0125	0.012	0.125
VBrotF1	0.232	1.0
VBrotF09	0.209	0.9
VBrotF075	0.174	0.75
VBrotF05	0.116	0.5
VBrotF04	0.093	0.4
VBrotF025	0.058	0.25
VBrotF0125	0.029	0.125
VBrotF005	0.012	0.05
vrQ01F05	0.095	-
vrQ01F02	0.036	-
vrQ001F05	0.036	-

the kinematical properties and the importance of pursuing observational studies of cluster internal kinematics. The outline of the paper is the following: in Section 2 we describe method and initial conditions, in Section 3 we present our results, and in Section 4 we summarize our conclusions.

2 METHOD AND INITIAL CONDITIONS

The N -body simulations presented in this paper were carried out using the NBODY6 code (Aarseth 2003) accelerated by a GPU (Nittadori & Aarseth 2012), and run on the BIG RED II cluster at Indiana University.

Clusters are assumed to be on circular orbits in the host galaxy tidal field modeled as a point-mass, and the equations of motion are solved in a frame of reference co-rotating with the cluster around the host galaxy centre (see e.g. Heggie & Hut 2003). For all the simulations we consider systems with $N = 16,384$ equal-mass particles; particles moving beyond two times the Jacobi radius, r_J , are removed from the simulation. All the simulations are run until half of the initial cluster mass is lost; we have run 4 different random realizations of the initial conditions of each of the models to provide an indication of the extent of stochastic variations in the results.

For the initial conditions we consider three sets of models characterized by different structural and kinematical properties. The first set of simulations follow the evolution of isotropic King models (1966) with dimensionless central potential $W_0 = 7$ and different values of the filling factor, defined as the ratio of the half-mass radius to the Jacobi radius r_h/r_J or equivalently, the ratio of the model truncation radius to the Jacobi radius r_t/r_J (see Table 1).

For the second set of models we have considered a series of rotating initial conditions, sampled from the equilibria introduced by Varri & Bertin (2012). This family of distribution function-based models was specifically designed to describe quasi-relaxed stellar systems with finite total angular momentum, and the resulting configurations are characterized by differential rotation, approximately rigid in the centre and vanishing in the outer parts, and by pressure anisotropy. Specifically, as a result of the chosen trunca-

tion prescription of the distribution function in phase space and the requirement of self-consistency of the associated density-potential pair, the velocity dispersion tensor of the models is characterized by isotropy in the central region, weak radial anisotropy in the intermediate regions, and tangential anisotropy in the outer parts. For a complete description we refer the reader to Varri & Bertin (2012), here we just recall that the models are defined by four dimensionless parameters, with the concentration parameter W_0 (defined as the depth of the dimensionless potential well at the centre of the system), and a parameter $\hat{\omega}$ measuring the strength of the rotation, playing the leading roles. The additional parameters \bar{b} and c are determined by the analytical expression of the distribution function, and they determine the shape of the rotation radial profile.

The rotating models selected for this investigation are characterized by the following values of the dimensionless parameters: $W_0 = 6$, $\hat{\omega} = 0.25$, $\bar{b} = 0.05$, and $c = 1$. Such a choice is inspired by results of a first comparison between the Varri & Bertin (2012) models and selected Galactic globular clusters (the properties of the best-fit models of 47 Tuc, ω Cen, and M15, are available in Tables 3, 4 of Bianchini et al. 2013). The coupling between the angular momentum vectors associated with the internal rotation and the orbital motion is a non-trivial aspect of the definition of our initial conditions. For simplicity, in our current set-up the rotation axis is set to be perpendicular to the orbital plane and the cluster internal rotation is prograde (with respect to the orbital motion). As in the previous set of simulations, also in this case we have explored several different values of the initial filling factor (see Table 1). The dynamical interplay between internal rotation and external tidal field is a very rich field of investigation, which, so far, has been only partially explored (see e.g. Ernst et al. 2007; Hong et al. 2013). Indeed, this set of simulations is only a part of an extended survey aimed at studying the role of rotation in the long-term dynamical evolution of tidally limited rotating star clusters (Tiongco et al., in prep.).

The third set of simulations follow the evolution of models initially undergoing a phase of violent relaxation in the host galaxy external tidal field with different initial values of the virial ratio, $Q = T/|V|$ (where T and V are the system kinetic energy and potential energy respectively), and different ratios of the initial cluster limiting radius to the Jacobi radius (r_L/r_J). We use the following parameters for the initial conditions of the violent relaxation phase: (ID, Q , r_L/r_J): (vrQ01F05, 0.1, 0.5), (vrQ01F02, 0.1, 0.2), and (vrQ001F05, 0.01, 0.5). The systems are initially spherical and homogeneous. During the violent relaxation phase, the models develop an isotropic core, radial anisotropy in the intermediate regions, and either isotropic or tangentially anisotropic outer regions. The kinematical properties emerging at the end of the violent relaxation are qualitatively similar to those discussed in Vesperini et al. (2014); in this paper we focus on the *long-term* evolution of these systems. For these simulations the properties reported in Table 1 are those of the equilibrium systems at the end of the violent relaxation phase (averages of 4 realizations). We refer to the equilibrium properties of these systems as our initial conditions for the long-term evolution. These simulations were started with a slightly larger number of particles in order to take into account of the early loss of stars during the violent relaxation phase. At the end of the violent relaxation phase the vrQ01F05, vrQ01F02, and the vrQ001F05 systems had, respectively, 14,860, 16,297, and 17,091 particles (averages of 4 realizations).

To measure the anisotropy we use the ratio of the projected tangential to the radial velocity dispersion, σ_T/σ_R , measured on the cluster orbital plane. For the calculation of the velocity disper-

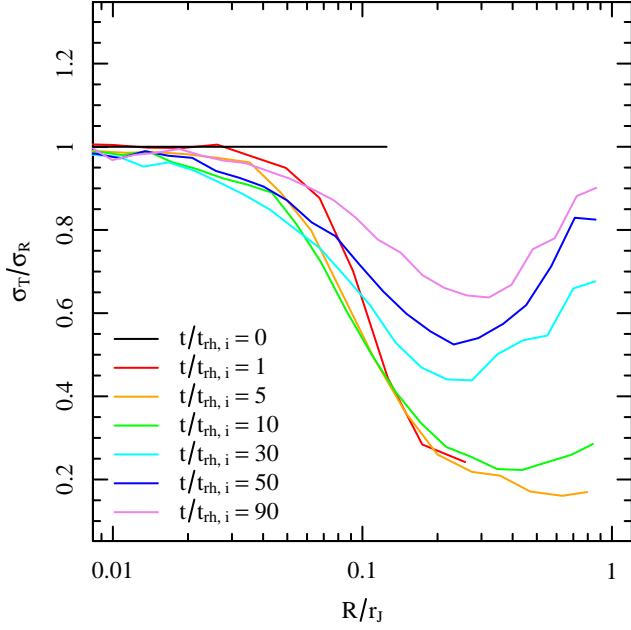


Figure 1. Time evolution of the radial profile of σ_T/σ_R for the model KF0125. The radius is normalized to the Jacobi radius, r_J . Each line is the median of the profiles obtained from the 4 realizations; see Section 2 for details. The theoretical isotropic profile of the King model at $t = 0$ is shown.

sions and their radial variation within the cluster, cylindrical shells along a line of sight perpendicular to the orbital plane with heights encompassing the entire cluster and at different projected radii, R , have been used. We have combined 5 snapshots around the desired times for each of the 4 realizations, then taking the profiles from each realization at the same times, calculated the median σ_T/σ_R at each R to get the median profile. We similarly find the upper and lower bounding profiles to represent the radial variation of the range of σ_T/σ_R . In the construction of the profiles all particles enclosed within the Jacobi radius have been taken into account.

3 RESULTS

3.1 Evolution of the velocity anisotropy

As shown in a number of studies (see e.g. Giersz & Heggie 1994a,b; Takahashi 1995, 1996, 1997; Spurzem & Aarseth 1996), during their long-term evolution initially isotropic and isolated star clusters develop a strong outer radial anisotropy. This feature may be easily interpreted as the orbital distribution in the halo being dominated by radial orbits, as a result of two-body relaxation in the cluster central regions. For tidally limited systems, on the other hand, the cluster structural evolution and expansion is limited by the tidal boundary, the growth of the radial anisotropy is suppressed by the preferential loss of stars on radial orbits resulting in an isotropic (or tangentially anisotropic) velocity distribution in the cluster outermost regions (see e.g. Takahashi et al. 1997; Takahashi & Lee 2000; Baumgardt & Makino 2003; Hurley & Shara 2012). As a cluster loses mass, its Jacobi radius will move toward the inner regions where the velocity dispersions are more isotropic, erasing the anisotropy that might have developed in the cluster intermediate regions (see Giersz & Heggie 1997).

We set the ground by examining in detail the time evolution

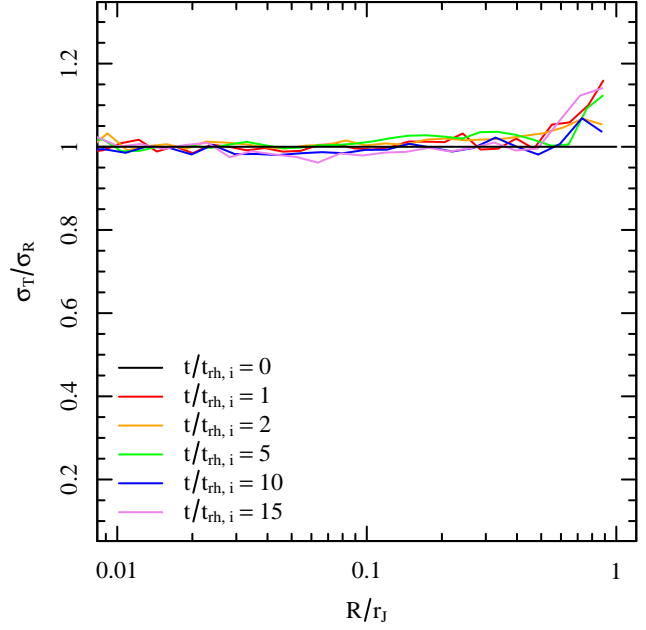


Figure 2. Same as Figure 1 for the model KF1.

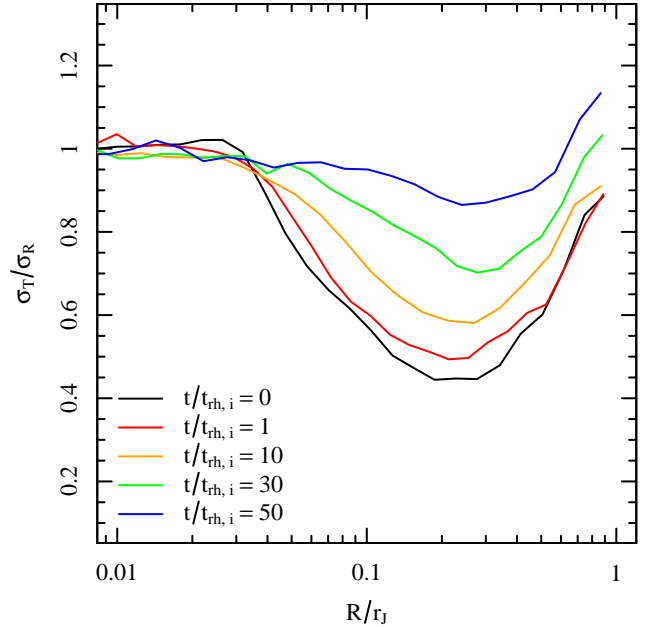


Figure 3. Same as Figure 1 for the model vrQ01F02.

of the radial anisotropy profile of two representative cases of the first set of simulations, i.e., the models starting from isotropic, non-rotating, King (1966) initial conditions. First, we consider the most underfilling case, with $(r_t/r_J)_i = 0.125$ (KF0125). As illustrated in Figure 1, the cluster is initially isotropic and underfilling, and, as it evolves and expands, it develops a strong radial anisotropy in the outer regions. As the system continues its evolution and starts to lose mass, a minimum in the anisotropy profile forms (corresponding to a maximum in the radial anisotropy) while the outermost regions become increasingly less radially anisotropic. This behavior is indeed consistent with the results of previous investigations based on N -body, Fokker-Planck, and gaseous methods discussed

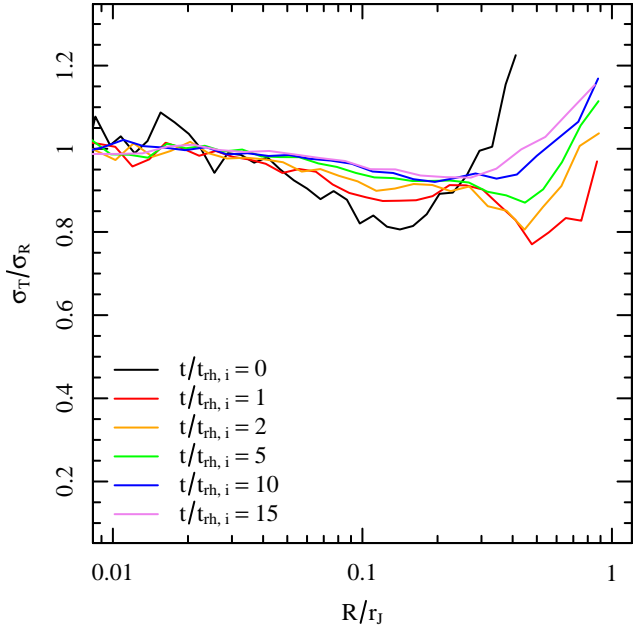


Figure 4. Same as Figure 1 for model VBrotF05.

at the beginning of this section. A similar radial variation in the velocity anisotropy is found in models based on the Michie-King distribution function (Michie 1963; see also Gieles & Zocchi 2015 for a recent study presenting a new family of anisotropic models). After this phase of the evolution, the overall strength of the radial anisotropy and the depth of the minimum will decrease. We will discuss in detail the evolution of the maximum radial anisotropy, its magnitude and location relative to the Jacobi radius over time as well as the dependence on the cluster initial conditions in Section 3.2.

We then continue the analysis of the first set of simulations by considering the tidally filling case, i.e. such that $(r_i/r_J)_i = 1$ (KF1). As depicted in Figure 2, such a tidally filling system never develops a significant degree of radial anisotropy, especially the outermost parts, which are instead characterized by (mild) tangential anisotropy. Such a behavior is consistent with the results of previous investigations by Baumgardt & Makino (2003). We emphasize that the development of such tangentiality is quite rapid (i.e., $t \sim 1 t_{rh,i}$), and it has been interpreted as a result of a preferential loss of stars on radial orbits in the outer parts of the systems, although the details of the processes underpinning such a behaviour are still only partly understood (see e.g. Keenan & Innanen 1975; Oh & Lin 1992). Further work to clarify the role of the loss of stars and of the external tidal field in the development of tangentiality is necessary.

A comparison between these two extreme cases clearly illustrates the importance of the initial filling factor of a system, and envisages the existence of a fundamental connection between a cluster kinematics and its initial properties and dynamical history. We will further discuss the implications of these differing kinematical signatures for clusters with different initial filling factors in Section 3.2.

It is now particularly instructive to move on to the third set of simulations, exploring the evolution of the products of violent relaxation in an external tidal field. Here our motivation was specifically to evaluate the long-term effects of the tidal perturbation, which was already responsible for having shaped the kinematic and

structural properties on the systems in the early phase of their dynamical evolution (for details, see Vesperini et al. 2014). As a representative case, in Figure 3 we examine model vrQ01F02, which is characterized by $Q = 0.1$ and $r_L/r_J = 0.2$, corresponding to intermediate values within the ranges explored in the third set of simulations.

Indeed, systems emerging from the violent relaxation phase start their long-term evolution with an anisotropy profile qualitatively similar to that produced on a much longer timescale in the underfilling KF0125 model (see Figure 3, black line corresponding to $t/t_{rh,i} = 0$), and the subsequent evolution is remarkably self-similar, driving the system toward a state characterized by a more isotropic orbital distribution (see Figure 3, blue line corresponding to $t/t_{rh,i} = 50$). Such an evolution is reflected in the decrease of the magnitude of the maximum of the radially-biased portion of the profile. The extent of the maximum radial anisotropy depends on the initial filling factor and virial ratio with colder and/or more underfilling initial conditions producing a stronger radial anisotropy (see also Vesperini et al. 2014).

Finally, we now consider the systems initially characterized by internal rotation, investigated in the second set of simulations. For our detailed analysis, illustrated in Figure 4, we focused on model VBrotF05 which, again, corresponds to an intermediate filling factor, among the values considered in this section of our investigation.

The initial conditions (see Figure 4, black line corresponding to $t/t_{rh,i} = 0$) have an isotropic core, a radially anisotropic intermediate region, and a tangentially isotropic outer region. We emphasize that, in this case, the initial radial anisotropy and the location of its maximum are *intrinsic* properties of the model adopted and not the result of the cluster early or late evolution. The location of the maximum anisotropy in the initial model is near the half-mass radius, and its location relative to the Jacobi radius will depend on the initial filling factor. We also point out that the strength of the intrinsic projected anisotropy of the rotating model depends on the angle between the line of sight and the rotation axis (it is larger when the line of sight is parallel to the rotation axis and decreases as the line of sight moves to a direction perpendicular the rotation axis). The shape of the anisotropy profile during the first 1-2 relaxation times will also depend on the initial filling factor. During the evolution of underfilling VBrot systems, the intrinsic anisotropy is erased while the system is expanding and its outer anisotropy evolution resembles that shown in Figure 1 for initially underfilling King models (see Figure 4, lines corresponding to $t/t_{rh,i} = 10, 15$). Underfilling models may be characterized by two minima in the profile at early times, the inner one being intrinsic to the model, and the outer one resulting from the cluster evolution (see the red line corresponding to $t/t_{rh,i} = 1$ in Figure 4). For the more filling VBrot systems, the model's intrinsic radial anisotropy is initially located near the range of radial distances where the anisotropy produced by evolution develops. Similarly to what happens for the more filling King models, these models develop only a mild tangential anisotropy in the outer regions during their evolution.

3.2 Properties of the maximum radial velocity anisotropy

In the previous section we have illustrated how differences in a cluster initial conditions and evolutionary phases can affect the evolution of a cluster kinematics and leave different fingerprints in the anisotropy radial profile. In this section, we further explore the connection between initial conditions, dynamical evolution and radial anisotropy by focusing our attention on the strength of the max-

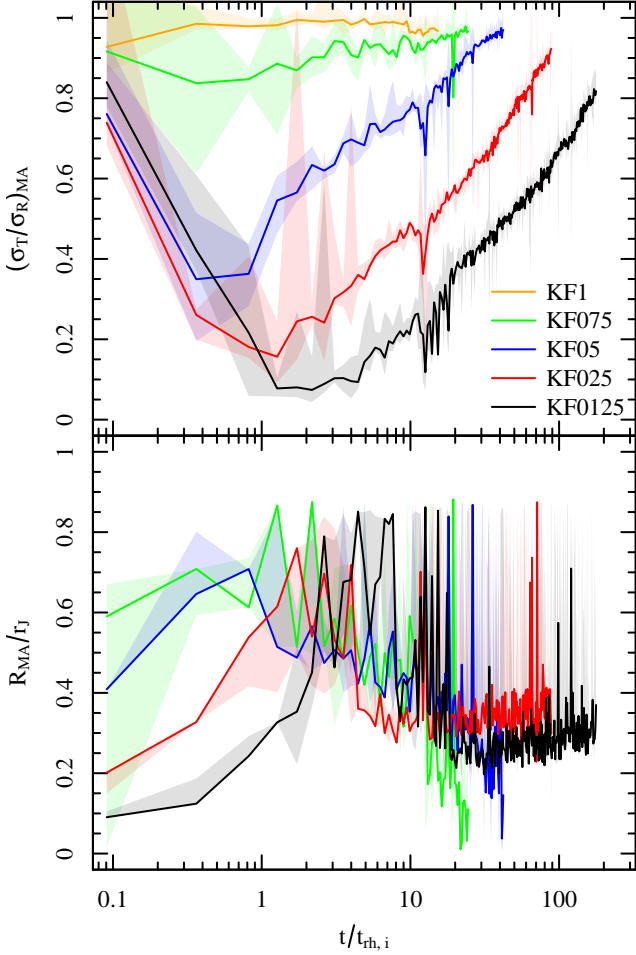


Figure 5. Top Panel: Time evolution of the value of the maximum radial anisotropy for the isotropic King models. The solid line is, for each time, the maximum anisotropy of the median profile (see Section 2 for explanation and Figures 1-4 for examples), while the upper and lower bounds represent the range of the anisotropy of the 4 realizations at that location. Bottom panel: Evolution of the location of the maximum radial anisotropy relative to the Jacobi radius. The solid line, upper, and lower bounds represent the location of the maximum anisotropy for the median, upper, and lower bounding profiles at each time for the 4 simulations. The line for KF1 is omitted from the bottom panel because this model never develops a significant radial anisotropy.

imum radial anisotropy, $(\sigma_T/\sigma_R)_{MA}$, and its location, R_{MA} . We show in Figures 5-7 the time evolution $(\sigma_T/\sigma_R)_{MA}$ and R_{MA} , relative to the Jacobi radius for each set of models. More underfilling initial conditions develop stronger radial anisotropy while, for all systems, the location of the maximum radial anisotropy is between 0.2 and 0.4 r_J for most of the cluster's lifetime.

As for the time evolution of R_{MA} we point out that, as was shown in Figure 1, the rising portion of the anisotropy profile appears only after the system expanded to the outermost regions approaching the Jacobi radius. The development of this feature in the anisotropy radial profile corresponds to the time when R_{MA}/r_J stops increasing and $(\sigma_T/\sigma_R)_{MA}$ stops decreasing (see Figure 5). Figure 5 clearly shows the connection between a cluster initial filling factor and the strength of the radial anisotropy developed during its dynamical evolution: initially compact clusters with smaller initial filling factors develop stronger radial anisotropy. Only during

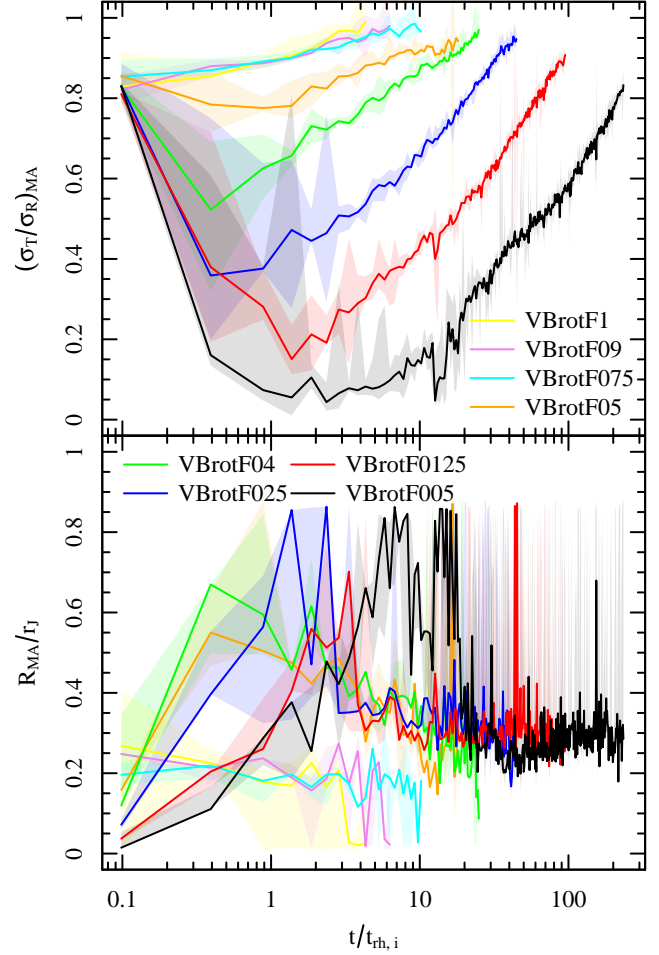


Figure 6. Same as Figure 5 for the VBrot models.

the late stages of their evolution when they have lost a significant fraction of their mass, underfilling systems evolve toward a more isotropic velocity distribution (we emphasize that we refer here to mass loss occurring during the cluster long-term evolution and due to two-body relaxation not to early mass loss due to stellar evolution). This point is further illustrated in Figure 8 which shows the evolution of the maximum radial anisotropy as a function of mass lost for several underfilling models. Underfilling systems develop a strong radial anisotropy which is gradually erased as the cluster evolves and loses mass. Our simulations show that clusters which are initially significantly underfilling should now be characterized in their intermediate regions by a strong radial anisotropy unless they are in the very advanced stages of their evolution and have lost a significant fraction of their initial mass. Many clusters should not have suffered such a strong relaxation-driven mass loss and information on their initial structural properties should therefore be imprinted in the strength of the radial anisotropy in their outer regions.

Figure 6 shows the time evolution of R_{MA} and $(\sigma_T/\sigma_R)_{MA}$ for the VBrot models. As discussed in Section 2 these models are characterized by an initial intrinsic maximum in the radial anisotropy. Therefore, the initial radial location of the maximum anisotropy relative to the Jacobi radius depends on the initial filling factor and, in general, does not fall in the range of values ($R_{MA}/r_J \sim 0.2 - 0.4$) typical for the maximum anisotropy pro-

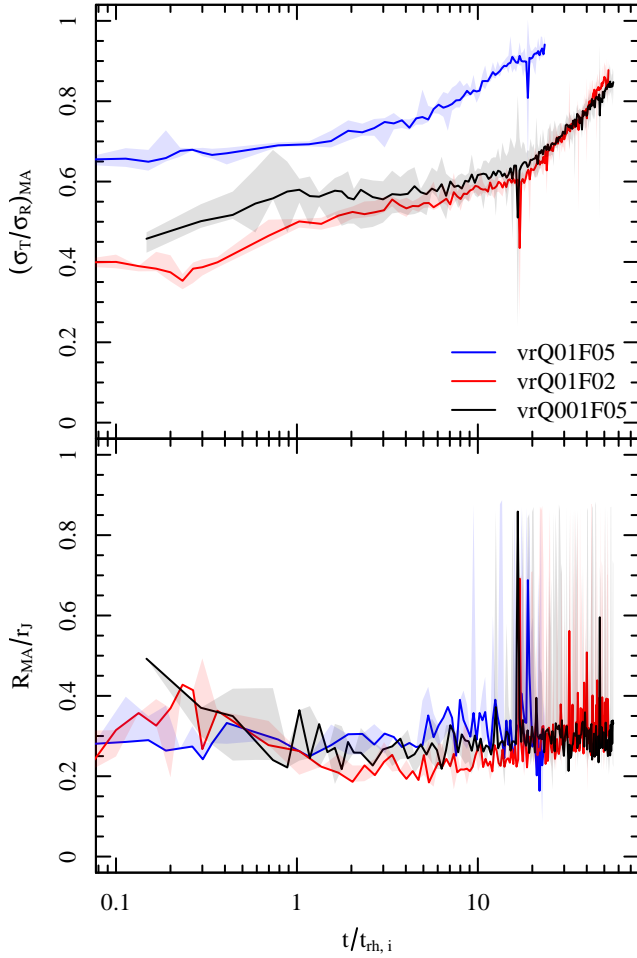


Figure 7. Same as Figure 5 for the vr models.

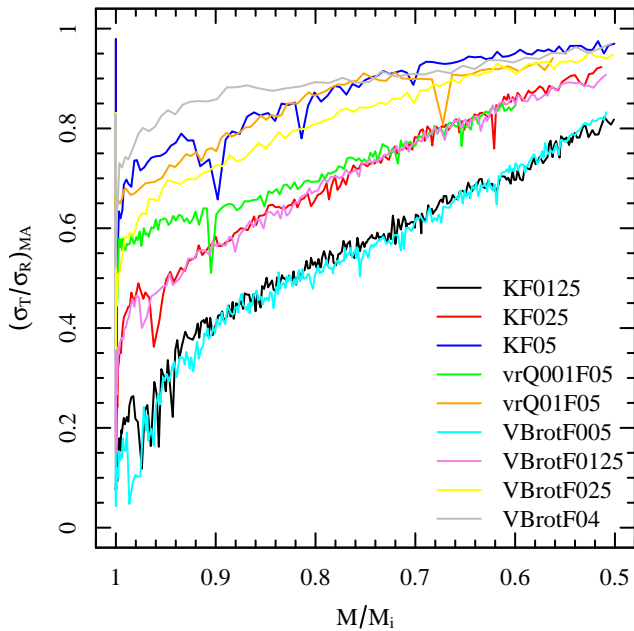


Figure 8. Evolution of the value of the maximum radial anisotropy as function of fraction of initial mass remaining for several models.

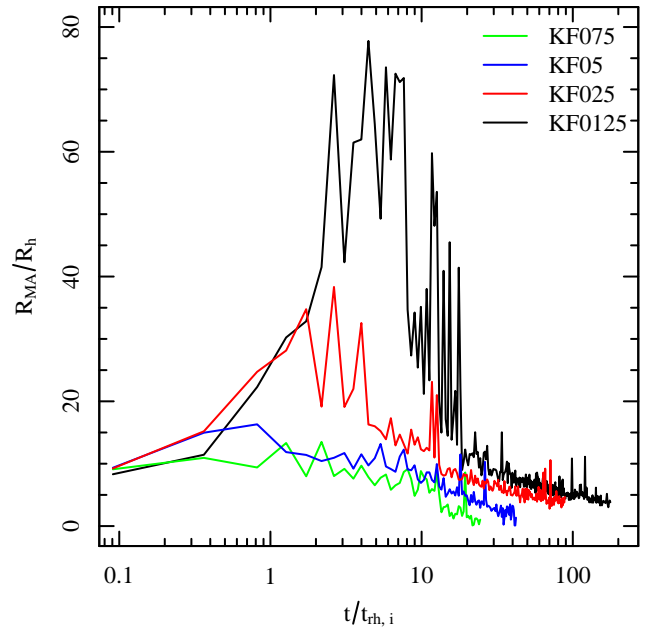


Figure 9. Evolution of R_{MA} in terms of the projected half-mass radius, R_h for the King models.

duced by early or long-term dynamical evolution. Only for the initially more filling models the intrinsic maximum radial anisotropy is at $0.2-0.3 r_J$. For underfilling models, the maximum radial anisotropy rapidly (within $1 t_{rh,i}$) transitions from the intrinsic maximum to the one developed in the outermost regions of the cluster as it expands (see for example the radial profile of σ_T/σ_R at $t/t_{rh,i} = 1$ in Figure 4). For the most filling models (VBrotF075, VBrotF09, and VBrotF1) dynamical evolution does not produce a significant radial anisotropy; for these models, Figure 6 shows the gradual erasing of the intrinsic anisotropy.

The vr models also begin their long-term evolution with a velocity distribution characterized by a region of significant radial anisotropy produced early during the cluster violent relaxation phase and the radial position of the maximum radial anisotropy falls between $0.2-0.4 r_J$. The evolution of $(\sigma_T/\sigma_R)_{MA}$ and R_{MA} for these models is similar to that found for the King models after the development of a minimum in the σ_T/σ_R radial profile. Figure 7 shows that for the vr models the maximum radial anisotropy will decrease over time while R_{MA} will generally remain between 0.2 and $0.4 r_J$.

3.3 Evolution of the anisotropy at R_h

The results presented in the previous section show that for the models developing a significant radial anisotropy the location of the maximum radial anisotropy falls in the range $0.2-0.4 r_J$ for most of a cluster's lifetime; as shown in Figure 9, this range can correspond to a distance of many half-mass radii from the cluster centre. On the observational side, anisotropy measurements in globular clusters do not cover, in most cases, distances larger than about $1-2$ half-mass radii, and the deviations from isotropy found are modest (see e.g. the results of the Hubble Space Telescope Proper Motion (HSTPROMO) catalogs of Galactic Globular Clusters: Bellini et al. 2014 and Watkins et al. 2015, where the values of σ_T/σ_R at the half-mass radius of radially anisotropic clusters are equal to about $0.9-0.95$ for the most radially anisotropic systems).

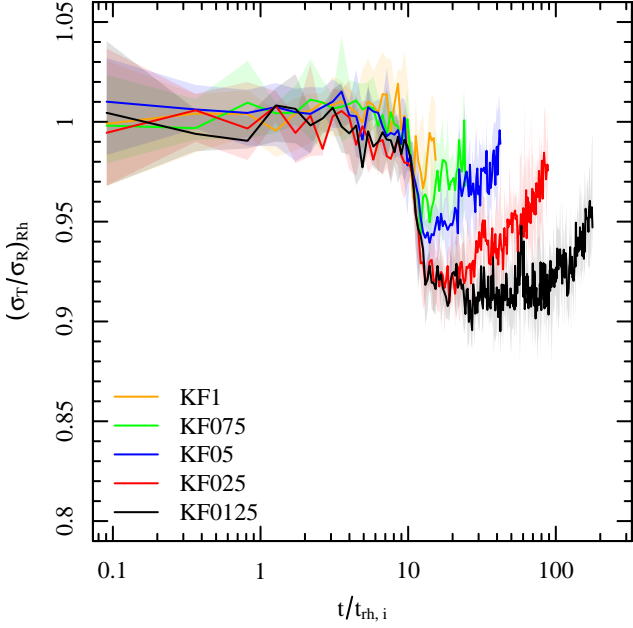


Figure 10. Evolution of the anisotropy at R_h for the King models.

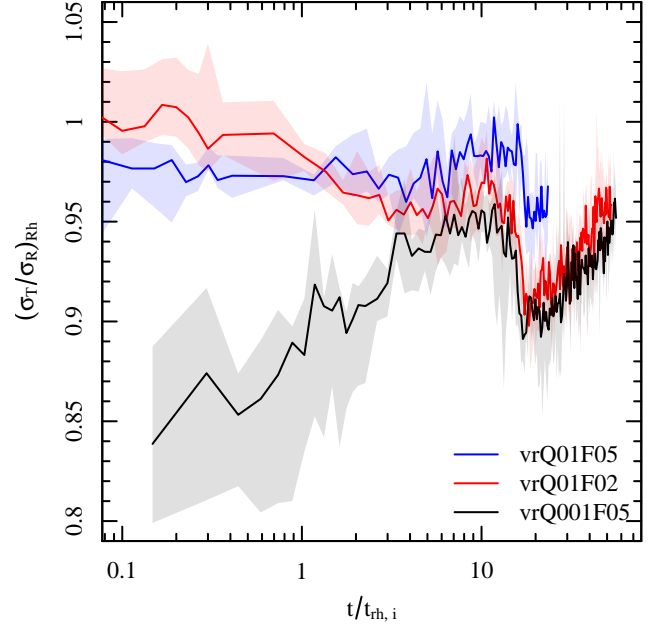


Figure 12. Evolution of the anisotropy at R_h for the vr models.

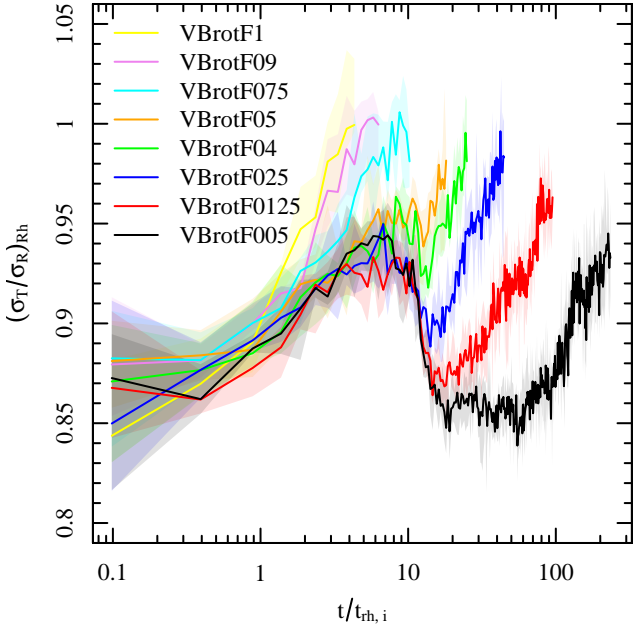


Figure 11. Evolution of the anisotropy at R_h for the VBrot models.

Motivated by these observational constraints, we have also evaluated the time evolution of the anisotropy measured at R_h for all models of our survey. As illustrated in Figures 10–12, models that are initially radially anisotropic (i.e., VBrot and vr models) become more isotropic over time, although there is a short time interval characterized by a rapid increase in radial anisotropy at the time of core collapse. After core collapse, all the systems investigated evolve again towards isotropy. For the VBrot models the anisotropy in the initial phase of evolution ($t \lesssim 2 t_{\text{rh},i}$) is that associated to the intrinsic anisotropy of the rotating models (as already pointed out in Section 3.1, the strength of the intrinsic projected anisotropy for the VBrot models depends on the angle between the

line of sight and the rotation axis. Figure 11 shows the values measured along a line of sight parallel to the rotation axis; for a 45 (90) degree angle, for $t \lesssim 2 t_{\text{rh},i}$, σ_T/σ_R at R_h is equal to about 0.95 (1)).

Figure 13 shows the evolution of σ_T/σ_R at a few different distances from the cluster centre for some of the models investigated in this paper. These figures provide a more comprehensive picture of the radial dependence of the anisotropy and its time evolution. A comparison of the models in Figure 13 further illustrates how the outer region kinematics may provide key fingerprints of a cluster evolution and initial structural properties. Specifically, as already pointed out above and in Section 3.1, initially underfilling systems and systems undergoing an early violent relaxation phase should be characterized by a strong radial anisotropy in their outer regions unless they are in the advanced stages of their evolution and have lost a significant fraction of their initial mass. Finally, in Figure 13 we also show the anisotropy measured along two different lines of sight and find no significant differences depending on the line of sight.

4 CONCLUSIONS

In this paper we have presented the results of an extensive survey of N -body simulations aimed at exploring the long-term evolution of the velocity anisotropy in tidally limited star clusters. We have studied the evolution of three sets of models characterized by different initial structural and kinematical properties: isotropic King models (King 1966), rotating systems described by the models introduced by Varri & Bertin (2012), and systems starting with a core-halo structure and kinematical properties imprinted by an early phase of violent relaxation in an external tidal field.

We have explored in particular the dependence of the evolution of the anisotropy and its radial variation within a cluster on the initial filling factor (defined as the ratio of the cluster half-mass to Jacobi radius, r_h/r_J) and have shown that, in all three sets of models, this is a key parameter in determining the degree of radial

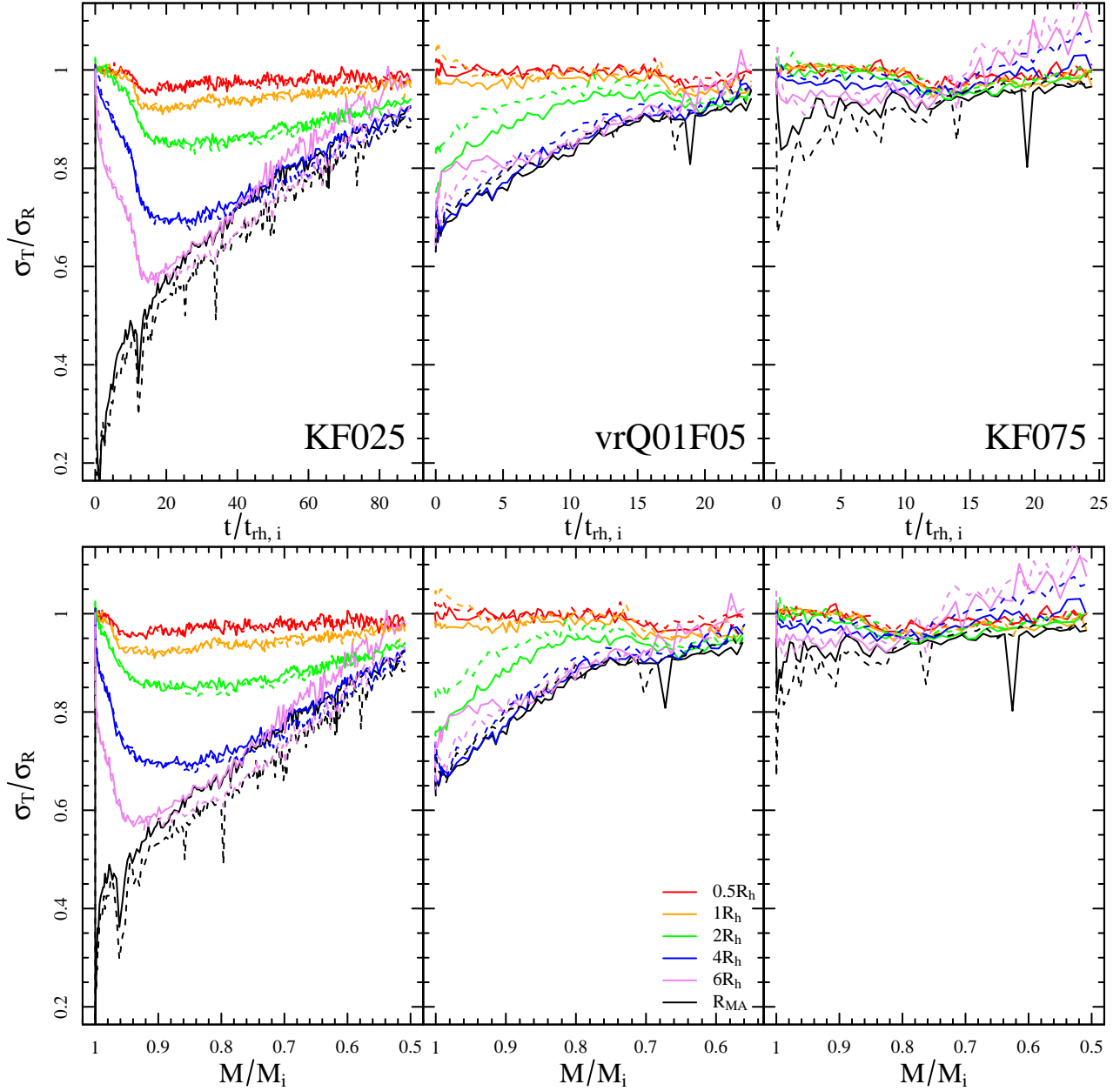


Figure 13. Evolution of the anisotropy at multiples of R_h for a few representative models. The top panels show the evolution as a function of time, and the bottom panels as a function of fraction initial mass remaining in the cluster. Solid lines show the profiles calculated, as in previous figures, as projected along a line of sight perpendicular to the orbital plane; dashed lines show the profiles calculated as projected along a line of sight parallel to the orbital plane of the cluster.

anisotropy that can develop in the intermediate and outer parts of a star cluster. Indeed, while the detailed evolution of the profile of the anisotropy as a function of radius show some differences in the three sets of simulations explored in this study, a global characteristic behavior clearly emerges.

First of all, clusters with smaller initial values of r_h/r_J develop a stronger radial anisotropy. In addition, while the strength of the maximum radial anisotropy developed during a cluster evolution strictly depends on the filling factor and the dynamical phase, its location within a cluster is approximately constant and falls in the range $0.2-0.4 r_J$ during most of the cluster evolution.

Systems starting from isotropic, underfilling initial conditions

during their evolution are typically characterized by an isotropic core followed by a region with an increasing radial anisotropy, determined by the build-up of radial orbits in the outer parts of the cluster, reaching a maximum between 0.2 and $0.4 r_J$ and then decreasing again and becoming isotropic or mildly tangentially anisotropic in the cluster outermost regions.

As a cluster evolves and starts to lose mass, the growth of the radial anisotropy eventually stops and the systems evolves again toward an isotropic velocity distribution at all distances from the cluster centre. However such a global isotropic velocity distribution is expected only for systems in the advanced stages of their evolution after they have lost a significant fraction of their initial mass (we

emphasize that we refer here to long-term mass loss due to two-body relaxation not to the early mass loss due to stellar evolution). Smaller initial values of r_h/r_J lead to stronger radial anisotropy and require a larger amount of mass loss before their velocity distribution becomes isotropic again.

On the other hand, it is crucial to recognize that initially isotropic, tidally filling systems never develop a significant radial anisotropy.

Interestingly, the behavior described above apply also to stellar systems starting from initial conditions characterized by moderate rotation and mild deviations from isotropy in the velocity space.

As for star clusters undergoing an early phase of violent relaxation in an external tidal field, we show that, as previously found in Vesperini et al. (2014), these systems quickly develop during this phase an anisotropy profile similar to that described above (an isotropic core followed by regions with an increasing radial anisotropy reaching its maximum at $\sim 0.2-0.4 r_J$ and then by isotropic or mildly tangentially anisotropic outermost regions). During their long-term evolution these systems become more isotropic but the anisotropy produced in their early evolution is, also in this case, erased only after they have lost a significant fraction of their initial mass.

The results of our simulations clearly show that information on the initial structural properties and dynamical history should be imprinted in the strength of the anisotropy in the intermediate and outer regions of stellar systems. Provided that a star cluster has not yet experienced severe mass loss, such information should be accessible for many Galactic globular clusters.

Several studies attempting to reconstruct the initial structural properties of a number of Galactic globular clusters have suggested that these systems might be initially characterized by small values of r_h/r_J (see e.g. Giersz & Heggie 2011; Gieles et al. 2011; Pijloo et al. 2015) and that many of them might not have lost a large fraction of their mass during their long-term evolution. A strong radial anisotropy in the intermediate/outer regions of these clusters is the expected kinematical fingerprint of the suggested initial conditions and dynamical phase of these clusters.

In addition to the obvious need to extend kinematical studies to a larger number of clusters, we emphasize the importance of extending the characterization of the degree of anisotropy to include star cluster intermediate and outer regions where, as shown by our results, the kinematical fingerprints of different initial conditions and dynamical history are expected to be stronger.

ACKNOWLEDGMENTS

This research was supported in part by Lilly Endowment, Inc., through its support for the Indiana University Pervasive Technology Institute, and in part by the Indiana METACyt Initiative. The Indiana METACyt Initiative at IU is also supported in part by Lilly Endowment, Inc. ALV acknowledges support from the Royal Commission for the Exhibition of 1851 and The Gruber Foundation in form of Research Fellowships.

REFERENCES

Aarseth S. J., 2003, *Gravitational N-Body Simulations*. Cambridge Univ. Press, Cambridge
 Anderson J., van der Marel R. P., 2010, *ApJ*, 710, 1032
 Baumgardt H., Makino J., 2003, *MNRAS*, 340, 227

Bellazzini M., Bragaglia A., Carretta E., Gratton R. G., Lucatello S., Catanzaro G., Leone F., 2012, *A&A*, 538, A18
 Bellini A., et al., 2014, *ApJ*, 797, 115
 Bellini A., et al., 2015, *ApJ*, 810, L13
 Bianchini P., Varri A. L., Bertin G., Zocchi A., 2013, *ApJ*, 772, 67
 Djorgovski S., Meylan G., 1994, *AJ*, 108, 1292
 Ernst A., Glaschke P., Fiestas J., Just A., Spurzem R., 2007, *MNRAS*, 377, 465
 Fabricius M. H., et al., 2014, *ApJ*, 787, L26
 Gebhardt K., Pryor C., Williams T. B., Hesser J. E., 1995, *AJ*, 110, 1699
 Gieles M., Heggie D. C., Zhao H., 2011, *MNRAS*, 413, 2509
 Gieles M., Zocchi A., 2015, *MNRAS*, 454, 576
 Giersz M., Heggie D. C., 1994a, *MNRAS*, 268, 257
 Giersz M., Heggie D. C., 1994b, *MNRAS*, 270, 298
 Giersz M., Heggie D. C., 1997, *MNRAS*, 286, 709
 Giersz M., Heggie D. C., 2011, *MNRAS*, 410, 2698
 Gunn J. E., Griffin R. F., 1979, *AJ*, 84, 752
 Heggie D., Hut P., 2003, *The Gravitational Million-Body Problem: A Multidisciplinary Approach to Star Cluster Dynamics*. Cambridge Univ. Press, Cambridge
 Hong J., Kim E., Lee H. M., Spurzem R., 2013, *MNRAS*, 430, 2960
 Hurley J. R., Shara M. M., 2012, *MNRAS*, 425, 2872
 Kacharov N., et al., 2014, *A&A*, 567, A69
 Keenan D. W., Innanen K. A., 1975, *AJ*, 80, 290
 King I. R., 1966, *AJ*, 71, 64
 Lanzoni B., et al., 2013, *ApJ*, 769, 107
 Lardo C., et al., 2015, *A&A*, 573, A115
 Lupton R. H., Gunn J. E., Griffin R. F., 1987, *AJ*, 93, 1114
 Lützgendorf N., Kissler-Patig M., Noyola E., Jalali B., de Zeeuw P. T., Gebhardt K., Baumgardt H., 2011, *A&A*, 533, A36
 McLaughlin D. E., van der Marel R. P., 2005, *ApJS*, 161, 304
 Meylan G., Heggie D. C., 1997, *A&ARv*, 8, 1
 Michie R. W., 1963, *MNRAS*, 125, 127
 Miocchi P., et al., 2013, *ApJ*, 774, 151
 Nitadori K., Aarseth S. J., 2012, *MNRAS*, 424, 545
 Oh K. S., Lin D. N. C., 1992, *ApJ*, 386, 519
 Pancino E., Bellazzini M., Marinoni S., 2013, *Mem. Soc. Astron. Ital.*, 84, 83
 Pijloo J. T., Portegies Zwart S. F., Alexander P. E. R., Gieles M., Larsen S. S., Groot P. J., Devecchi B., 2015, *MNRAS*, 453, 605
 Pryor C., Meylan G., 1993, in Djorgovski S. G., Meylan G., eds, *ASP Conf. Ser. Vol. 50, Structure and Dynamics of Globular Clusters*. Astron. Soc. Pac., San Francisco. p. 357
 Richer H. B., Heyl J., Anderson J., Kalirai J. S., Shara M. M., Dotter A., Fahlman G. G., Rich R. M., 2013, *ApJ*, 771, L15
 Sollima A., Baumgardt H., Zocchi A., Balbinot E., Gieles M., Hénault-Brunet V., Varri A. L., 2015, *MNRAS*, 451, 2185
 Spurzem R., Aarseth S. J., 1996, *MNRAS*, 282, 19
 Takahashi K., 1995, *PASJ*, 47
 Takahashi K., 1996, *PASJ*, 48, 691
 Takahashi K., 1997, *PASJ*, 49, 547
 Takahashi K., Lee H. M., 2000, *MNRAS*, 316, 671
 Takahashi K., Lee H. M., Inagaki S., 1997, *MNRAS*, 292, 331
 van Leeuwen F., Le Poole R. S., Reijns R. A., Freeman K. C., de Zeeuw P. T., 2000, *A&A*, 360, 472
 Varri A. L., Bertin G., 2012, *A&A*, 540, A94
 Vesperini E., Varri A. L., McMillan S. L. W., Zepf S. E., 2014, *MNRAS*, 443, L79
 Watkins L. L., van der Marel R. P., Bellini A., Anderson J., 2015, *ApJ*, 803, 29